Single-cell measurement of red blood cell oxygen affinity

Giuseppe Di Caprio[a,1], Chris Stokes[a], John M. Higgins[b,c], and Ethan Schonbrun[a]

[a]The Rowland Institute, Harvard University, Cambridge, MA 02142; [b]Center for Systems Biology, Massachusetts General Hospital, Boston, MA 02115; and [c]Department of Systems Biology, Harvard Medical School, Boston, MA 02115

Edited by David A. Weitz, Harvard University, Cambridge, MA, and approved July 1, 2015 (received for review May 11, 2015)

Oxygen is transported throughout the body by hemoglobin (Hb) in red blood cells (RBCs). Although the oxygen affinity of blood is well-understood and routinely assessed in patients by pulse oximetry, variability at the single-cell level has not been previously measured. In contrast, single-cell measurements of RBC volume and Hb concentration are taken millions of times per day by clinical hematology analyzers, and they are important factors in determining the health of the hematologic system. To better understand the variability and determinants of oxygen affinity on a cellular level, we have developed a system that quantifies the oxygen saturation, cell volume, and Hb concentration for individual RBCs in high throughput. We find that the variability in single-cell saturation peaks at an oxygen partial pressure of 2.9%, which corresponds to the maximum slope of the oxygen–Hb dissociation curve. In addition, single-cell oxygen affinity is positively correlated with Hb concentration but independent of osmolarity, which suggests variation in the Hb to 2,3-diphosphoglycerate (2–3 DPG) ratio on a cellular level. By quantifying the functional behavior of a cellular population, our system adds a dimension to blood cell analysis and other measurements of single-cell variability.

hematology | medical sciences | flow cytometry | organ on chip | single-cell variability

Red blood cells (RBCs) are the most common type of blood cell and constitute approximately one-half of the human body's total cell count (1). They take up oxygen in the lungs and deliver it throughout the body, taking, on average, 20 s to complete one circuit through the circulation (2). Each cell is densely packaged with hemoglobin (Hb) that binds and releases oxygen based on the local oxygen partial pressure. The fraction of occupied binding sites relative to the total number of binding sites is called the oxygen saturation and can be described by the Hb–oxygen dissociation curve. Although it is known that several factors affect the oxygen affinity of Hb and consequently, shift the dissociation curve, such as pH, temperature, and 2,3-diphosphoglycerate (2–3 DPG) (3), it is not known how much variation these factors cause on a cellular level within individuals.

Recently, there has been significant progress in developing biomimetic environments for studying physiological processes of cells in vitro. Analogs to the lung (4), heart (5), bone marrow (6), and gut (7) have all been developed in microfabricated chips that enable ex vivo studies to closely replicate an in vivo environment. In addition to adherent cell cultures, chips for studying flowing blood have been developed that enable control of oxygen partial pressure with high spatial resolution (8–12). We take advantage of this new technology and combine it with a recently developed microfluidic cytometry method that enables us to quantify cell volume and Hb mass for individual flowing cells in high throughput (13).

Our system for measuring RBC mass is based on the optical absorption of Hb (14, 15). Unlike other recently developed single-cell mass measurements (16–20), however, it is straightforward to extend this method to resolving the mass of both oxygenated and deoxygenated species because of the well-known modification of the absorption spectra of Hb caused by oxygen binding (21). This method allows us to quantify RBC volume, Hb concentration (HbC), and oxygen affinity for cells while they are in a fluidic environment similar to the circulatory system. A few previous studies have explored the measurement of single-cell saturation (22–24), but to our knowledge, saturation measurements have never been performed on a large cell population or under accurate control of oxygen partial pressure.

In this paper, we first describe the physical properties of the microfluidic chip followed by the optical measurement system for obtaining cell volume and Hb mass. We then discuss the spectroscopic measurement system and the quantification of single-cell saturation from the measured multispectral absorption. The temporal dynamics of the system are then characterized to better understand the time and length scales required for equilibrium deoxygenation. We use our system to capture an Hb–oxygen dissociation curve and an SD curve as a function of oxygen partial pressure. At each oxygen partial pressure, we can retrieve a full distribution of single-cell oxygen saturation and observe its correlation to total HbC. In addition, using the measured saturation values, we can retrieve the oxygen partial pressure where the saturation is 50% (P_{50}) value for each cell in the population using the Hill equation as a model.

Functional RBC Analyzer

The microfluidic device to control the oxygen partial pressure and deliver cells to the measurement region is shown in Fig. 1 *A* and *B*. The device is composed of three layers: one layer in which the RBCs flow, a thin gas-permeable membrane in poly(dimethylsiloxane) (PDMS; thickness = 90 μm), and the gas layer (section shown in Fig. 1*B*). Cells are driven through the microfluidic device using a syringe pump and flow through a gas exchange region that is 1-cm long, 1-mm wide, and 6-μm thick. As they flow, cells

Significance

Oxygen transport is the most important function of red blood cells (RBCs). We describe a microfluidic single-cell assay that quantifies the oxygen saturation of individual RBCs in high throughput. Although single-RBC measurements of volume and mass are routinely performed in hospitals by hematology analyzers, measurements that characterize the primary function of RBCs, the delivery of oxygen, have not been made. With this system, we find measurable variation that is positively correlated with cellular hemoglobin concentration but independent of osmolarity. These results imply that the cytoplasmic environment of each cell is different and that these differences modulate the function that each cell performs.

Author contributions: G.D.C., J.M.H., and E.S. designed research; G.D.C. performed research; C.S. contributed new reagents/analytic tools; G.D.C. and E.S. analyzed data; and G.D.C., J.M.H., and E.S. wrote the paper.

The authors declare no conflict of interest.

This article is a PNAS Direct Submission.

[1]To whom correspondence should be addressed. Email: dicaprio@rowland.harvard.edu.

This article contains supporting information online at www.pnas.org/lookup/suppl/doi:10.1073/pnas.1509252112/-/DCSupplemental.

www.pnas.org/cgi/doi/10.1073/pnas.1509252112

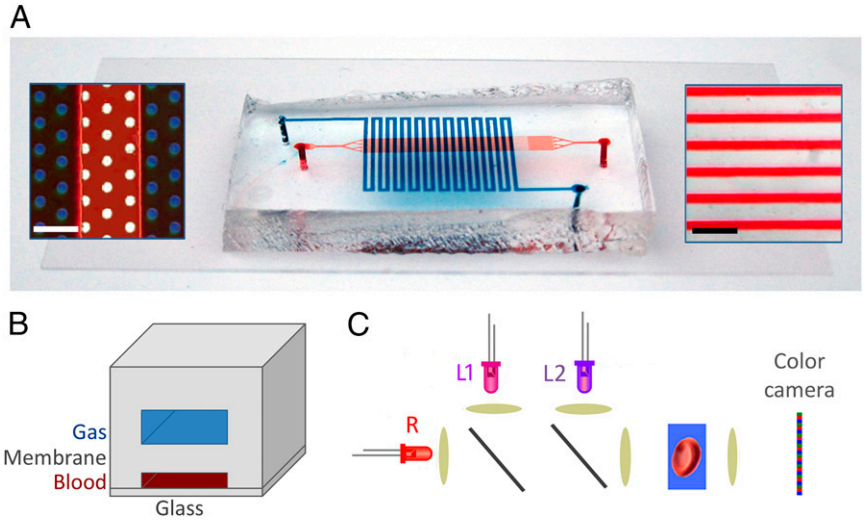

Fig. 1. Gas exchange RBC cytometry. *A* shows a side view of the microfluidic chip. The gas and the sample channel are filled with blue and red dye, respectively. The sample channel is 2.2-cm long. *Left Inset* shows a picture of the gas exchange region, where the pillar structure is visible as well as the overlay between the gas and the sample channel. *Right Inset* shows the parallel channels in the measurement region. (Scale bars: *Insets*, 200 μm.) (*B*) Sketch of the cross-section of the three layers composing the chip. *C* shows the optical setup. Two blue (L1 and L2) and one red (R) LEDs are combined using dichroic mirrors. The light transmitted by the cells flowing in the microfluidic channel is then projected onto a color camera by a microscope objective.

equilibrate with the oxygen partial pressure in the gas channel located above a gas-permeable membrane. A hexagonal lattice of PDMS pillars (50-μm diameter separated by 100 μm) sustains the channel (Fig. 1*A*, *Left Inset*). Traveling at a mean velocity of 2 mm/s, cells spend ~5 s in the gas exchange region, which is comparable with the time that they spend in the microcirculation (25). The gas channel is serpentine and has dimensions of 250-μm wide and 35-μm thick. The oxygen partial pressure of the input gas is controlled off chip by mixing a tank of pure N_2 with a tank of air (21% O_2 and 79% N_2). The partial pressure of the gas mixture is measured by an oxygen sensor (GS-Yuasa Oxygen Sensors KE-Series) before and after flowing in the gas serpentine channel to verify that the system has reached a steady-state condition. After cells pass through the gas exchange region, they are imaged in the measurement region, which is composed of 16 parallel channels (width of 30 μm) shown in Fig. 1*A*, *Right Inset*. Cells are measured within 100 μm of the last gas channel to minimize reoxygenation, and we have verified that oxygen saturation values in this region are similar to those measured underneath the last gas channel itself.

The optical setup is shown in Fig. 1*C*. Cells are suspended in a refractive index-matching buffer, into which a nonmembrane-permeable absorbing dye has been added (AB9; concentration of 0.8 g/dL) (13, 26). The cells are illuminated using a red light-emitting

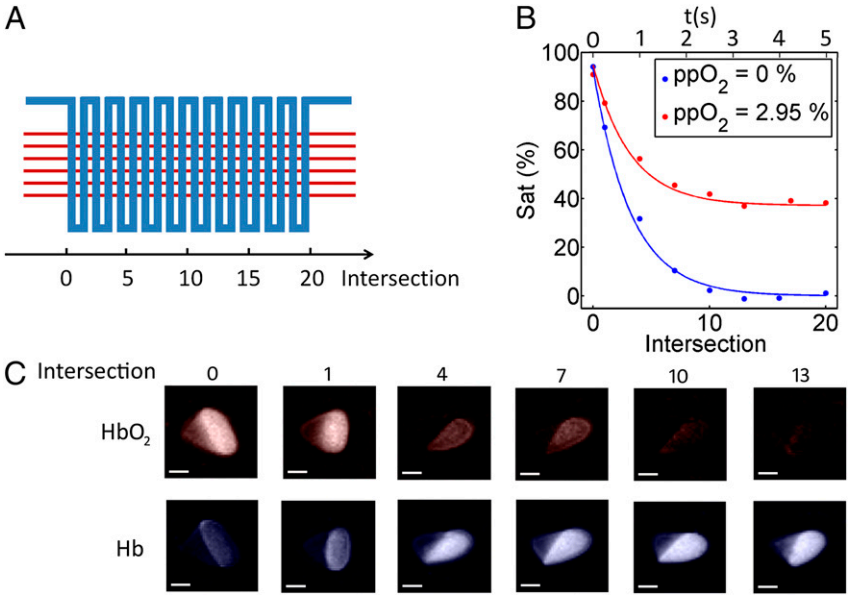

Fig. 2. RBC oxygen binding kinetics. *A* shows a schematic of the chip geometry used to characterize cellular binding kinetics. Blood flows in the red straight channel from left to right, and the saturation is measured at different intersections with the gas channel (in blue). *B* shows the saturation (Sat) at different intersections for two different gas mixtures plotted vs. intersection number and time for a cell velocity of 2 mm/s. (*C*) HbO_2 and Hb mass maps of flowing cells at different intersections. (Scale bar: 3 μm.)

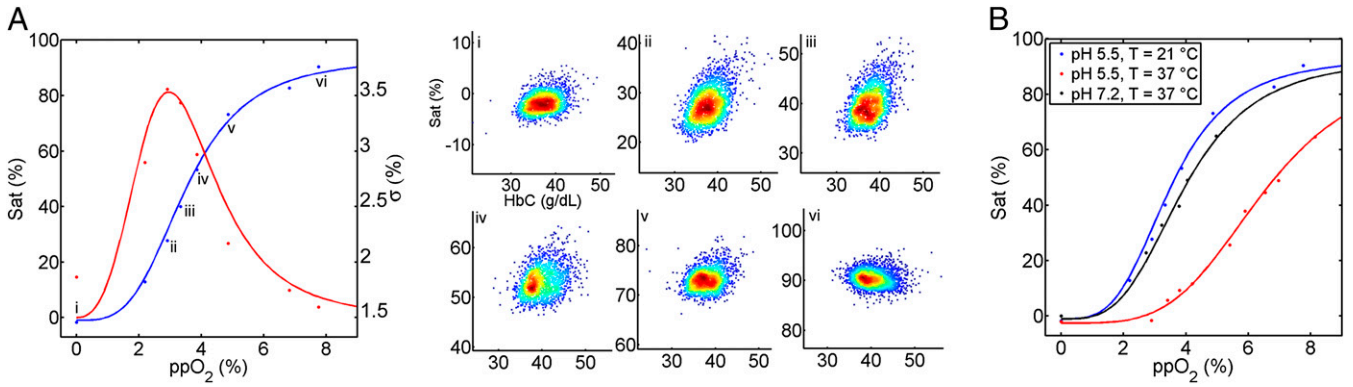

Fig. 3. Single-cell saturation distribution. *A* shows the mean (blue points) and SD (red points) of measured saturation at different values of ppO_2. The blue and red lines plot the Hill function and its derivative fitting the saturation values and the SD, respectively. (*A*, *i–vi*) Scatter plots of saturation vs. HbC for six different ppO_2 are shown. (*B*) Saturation values and the dissociation curves measured for different pH values and temperatures. The curves show the Hill function fits performed on the three sets of data. ppO_2 values at *i–vi* are 0%, 2.90%, 3.34%, 3.86%, 4.86%, and 7.76%, respectively. Sat, saturation.

diode (LED; λ = 625 nm) to quantify cell volume. The presence of a cell in the detection region displaces dye molecules in the optical path and consequently, increases the transmitted light signal. If there is minimal absorption or scattered light from the cell, the change in optical transmission can be related to the absolute cell height at each pixel of the image. The refractive index of the buffer has been increased to approach the average cell refractive index by adding 33 g/dL BSA. To quantify total Hb mass, which is the sum of oxygenated Hb (HbO_2) plus deoxygenated Hb mass, we use our previously shown method of quantitative absorption cytometry (13). HbO_2 and Hb have different absorption spectra. Consequently, by acquiring images of the same cell at wavelengths corresponding to the two absorption peaks (L1 and L2 in Fig. 1*C*), the two species of Hb in the cell can be decoupled and quantified (*Experimental Procedures*). Single-cell saturation is defined as the ratio of HbO_2 divided by the total Hb mass.

Kinetics of Oxygen Binding and Release

Because our goal in this study is to measure the oxygen saturation of cells that are at equilibrium with their environment, we need to first characterize the oxygen binding kinetics of flowing RBCs. For this measurement, we use a slightly different chip geometry, shown in Fig. 2*A*, where cells flow in straight channels for the entire duration of the gas exchange, which enables the oxygen binding and release kinetics to be studied. By measuring the value of the saturation at different intersections of the blood channel within the gas serpentine channel, we can quantify at what location and time the cells reach a stable oxygen saturation.

The mean cell saturation is shown at eight different positions for two gas mixtures of different partial pressures of oxygen (ppO_2 = 0% and 2.95%), with the mean cell saturation reaching equilibrium at 0% and 40%, respectively (Fig. 2*B*). It is evident from the plotted data that cells reach a stable saturation at around the 10th intersection. To further quantify the kinetics, we have fit the data using the decay function $\mathrm{Sat} = Ae^{(-x/\tau)} + B$ (Fig. 2*B*). As a function of the intersection number, we obtain a decay constant of τ = 3.2. Making use of the average cell velocity, we obtain a deoxygenation decay time of τ = 800 ms, which is comparable with the time that cells spend in the lung alveoli (25). For measurements taken beyond the 10th intersection, we have found no correlation between cell saturation and cell velocity or cell position. We consequently believe that, in the final measurement region, all cells are at a steady-state saturation and experience the same oxygen partial pressure. This condition results in variation of cell saturation that is caused exclusively by the variants of Hb that are in each cell and the cell's unique cytosolic environment. Fig. 2*C* shows the HbO_2 and Hb mass maps of different cells as a function of the intersection number at 0% ppO_2. From these images, it is also clear that cells have a constant oxygen saturation after the 10th intersection.

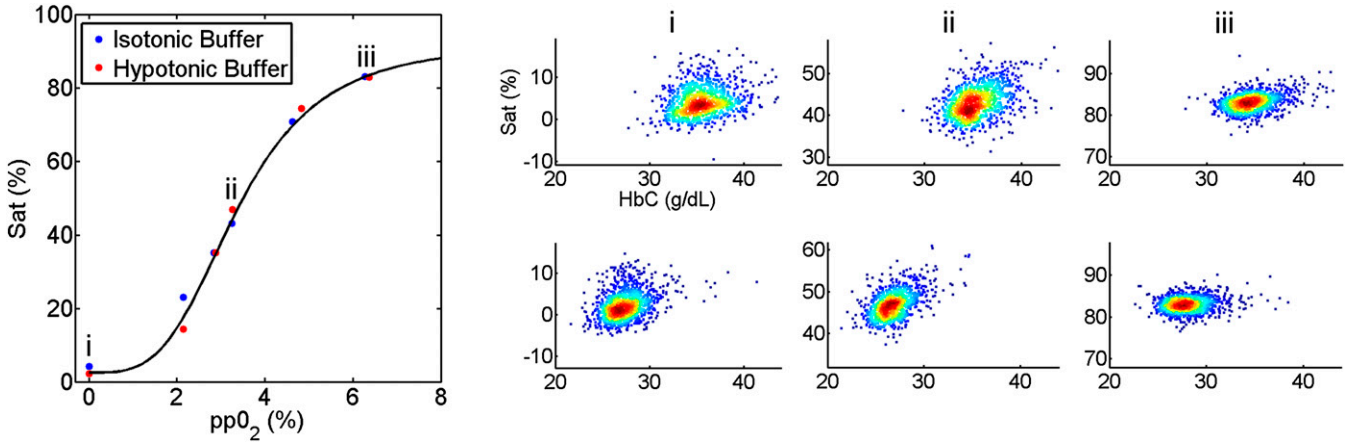

Fig. 4. Single-cell saturation and HbC. The plot shows saturation values for cells suspended in an isotonic (272 mOsm) and hypotonic (175 mOsm) buffer. The black line plots the Hill function fitting the saturation values in both regimes. Scatter plots of saturation vs. HbC for three different ppO_2 are showed for comparison between the two buffers with different osmolarity. ppO_2 values at *i–iii* are 0%, 3.25%, and 6.28%, respectively. Sat, saturation.

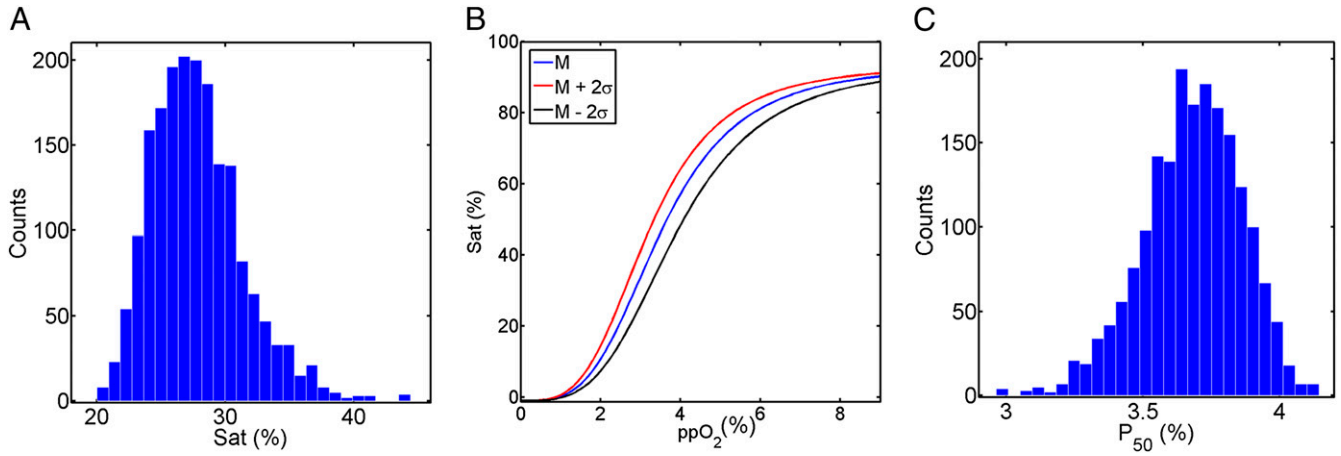

Fig. 5. Single-cell P_{50} distribution. *A* shows the saturation distribution at $ppO_2 = 2.92\%$, saturation mean (M) is 27.8%, and σ is 3%. *B* shows M (blue) and the values M + 2σ (red) and M − 2σ (black) at $PO_2 = 2.92\%$. *C* shows the corresponding P_{50} distribution, where the mean P_{50} is 3.68%. Sat, saturation.

Variability in Cellular Oxygen Affinity

By scanning ppO_2 from 0% to 21%, we can evaluate the mean and the SD (σ) of the single-cell saturation distribution as shown in Fig. 3*A* (plotted in blue and red, respectively). The curve of the mean saturation values is consistent with the expected cooperative binding model for Hb. To fit the mean saturation data, we use the Hill function (2)

$$\mathrm{Sat} = \frac{1}{\left(\frac{K_\mathrm{d}}{\mathrm{ppO_2}}\right)^{\mathrm{n}} + 1},$$

where K_d is a dissociation constant, and n is the Hill coefficient. The strength with which oxygen binds to Hb is affected by several factors, such as temperature, pH, Hb variants, and the ratio of 2–3 DPG to Hb. These data and the rest of the data in this paper (unless otherwise stated) were collected at 22 °C and pH 5.5 because of the acidic properties of BSA. For the curves plotted in Fig. 3*A*, the Hill coefficient is 3.5, and K_d is also 3.5. Fig. 3*B* shows the measured dissociation curve of the same sample under two other experimental conditions: one at physiological conditions of 37 °C and pH 7.2, where NaOH has been added to the buffer to neutralize the pH (measured using an ORION PerpHecT PH Meter), and one at 37 °C and pH 5.5. The sample at physiological conditions has a similar oxygen affinity, showing a slightly right shifted dissociation curve. The sample at 37 °C and low pH shows a substantially lower oxygen affinity, which is expected and caused by the Bohr Effect (2).

In addition to mean cell values, we can for the first time, to our knowledge, report σ of the saturation distribution as a function of oxygen partial pressure, which ranges from 1.2% to 2.9% when ppO_2 is 8% and 2.8%, respectively, for this sample. The low σ of 1.2% at 8% ppO_2 is expected, because the dissociation curve is almost flat at high pressures. We can consequently use this value (~1%) as a conservative estimate of the single-cell saturation measurement accuracy of our system. At each ppO_2, we analyze ~2,000 cells, and therefore, our estimated accuracy of the population mean is $\sigma/\sqrt{n} < 0.1\%$, which is similar to the uncertainty in SD for such a large sample size. Conversely, σ peaks when the slope of the dissociation curve is at its maximum, and at these pressures, the variation in saturation of different cells is at its maximum value. Interestingly, the cellular variation is much larger at venous than arterial ppO_2 (27). Across the entire range of pressure, we find that the SD curve is proportional to the slope of the dissociation curve, which we have used as a fit in Fig. 3*A*.

In addition to the mean and SD, we can plot the entire saturation distribution and investigate its correlation with RBC volume and HbC. Fig. 3*A* shows scatter plots of single-cell saturation and HbC for the same sample at six different ppO_2 values. As can be seen most easily in Fig. 3*A*, *ii* and *iii*, these two variables show an interesting positive correlation, where cells with high HbC show high saturation values. The measurement has been repeated on several different samples from different individuals, and each displays a positive correlation between HbC and cell saturation at pressures that correspond to the peak in variability. More details are in Fig. S1.

To further investigate the correlation of single-cell saturation with HbC, we perform measurements on the same sample in both an isotonic (272 mOsm) and a hypotonic (175 mOsm) buffer. If single-cell oxygen affinity is solely caused by cellular HbC, then one would expect the dissociation curve to shift when the HbC is reduced by the hypotonic buffer. We measured the mean HbC in the isotonic buffer to be 35.6 g/dL, whereas the mean HbC in the hypotonic buffer was reduced to 27.4 g/dL. As can be seen in Fig. 4, however, the same Hill function fits the saturation values in the isotonic and the hypotonic regimes. In addition, from the scatter plots, we see that, although the distribution of HbC shifts to the left in the hypotonic buffer, the shape and location of the cloud are maintained. It has been proposed that the oxygen affinity of Hb is modulated by its extremely high intracellular concentration in a process called molecular crowding, but this mechanism would produce a shift caused by the osmotic change in volume (28). Instead, we suspect that the observed correlation between HbC and cell saturation is caused by variation across the sample in the ratio between Hb and 2–3 DPG molecules inside each cell (29, 30). Osmotic perturbation will not change this ratio.

Although saturation values determine the oxygen content of a blood sample at a given ppO_2, it is often convenient to use a single number to quantify the oxygen affinity across a range of ppO_2. For this purpose, clinicians frequently use a blood sample's P_{50}. Using the Hill equation as a model, our measurement allows the evaluation of the P_{50} at a single-cell level. In Fig. 5*A*, we plot a histogram of the saturation distribution at $PO_2 = 2.92\%$ and the resulting P_{50} distribution. Fig. 5*B* shows the derived dissociation curves fitting the mean P_{50} (3.68%) in Fig. 5*B*, blue and the $\pm 2\sigma$ of P_{50} in Fig. 5*B*, red and black (3.34% and 4.08%, respectively). In each case, the fit has been performed by changing the dissociation constant and keeping the Hill coefficient constant. The P_{50} values reported in Fig. 5*C* show a good agreement to the ones reported in the literature [mean

P_{50} for a normal adult individual is 3.7% (2)]. The distribution is somewhat asymmetric, having a larger tail at low P_{50}. These high P_{50} cells have a greater oxygen affinity and will bind to oxygen in the lungs more efficiently, but they will be more reluctant to release oxygen to the tissues. Statistical analysis of the p50 distribution and its correlation with HbC can be found in Fig. S2.

Discussion

We have developed an optical measurement system that quantifies volume, Hb mass, and oxygen saturation for individual RBCs in high throughput, while simultaneously accurately controlling oxygen partial pressure. Delivering oxygen is the primary function of an RBC, and we believe this measurement could constitute a third RBC index in clinical hematology analysis along with single-cell volume and HbC (correlations of all three RBC indices are in Fig. S3).

Using this system, we have observed measurable differences in oxygen affinity on a cellular level. We have found that single-cell saturation is positively correlated with single-cell HbC but that oxygen affinity is not perturbed by changing the osmotic pressure. Instead of an intrinsic relationship between oxygen affinity and HbC, we believe that variability in single-cell oxygen saturation is caused by intercellular differences in the 2–3 DPG concentration. Oxygen affinity is modulated by the ratio of the number of 2–3 DPG molecules to the number of Hb molecules in each cell, which does not change under osmotic perturbation.

It is possible that some amount of variability in cellular oxygen affinity could be advantageous. There is a large gradient of ppO_2 across the body, and a distribution of cellular oxygen affinity could enable a more uniform delivery of oxygen. In addition, under hypoxic conditions, it may be valuable to have a subpopulation of cells with high oxygen affinity to transport oxygen at low ppO_2. It is also possible that too much variability is detrimental and could be used as a medical diagnostic for hematological disorders. Similarly, measurement of the P_{50} distribution for a cell population could yield valuable insights into the distribution of Hb variants that occur in various forms of anemia (31).

Although we have primarily focused in this paper on taking measurements of cells after they have reached equilibrium with their environment, the methods developed in this study will also be valuable for studying the binding kinetics of single cells before equilibrium has been reached. This measurement could enable a better understanding of the role of fluid dynamics in oxygen transport and the extent to which single-cell parameters affect these kinetics (32). It will also be valuable to quantify oxygen affinity under different temperatures and pH to better understand how these factors affect single-cell oxygen affinity and its regulation.

Experimental Procedures

Device Fabrication. The devices are fabricated using two separate masters, where each is lithographically patterned into SU8 photoresist (Microchem) on a silicon substrate. The mold with the blood flow channel is spin-coated with a 100-μm layer of PDMS prepolymer (1:10 mixture of base:curing agent of Sylgard 184 by Dow Corning spun at 1,000 rpm for 40 s) and partially cured for 3 h at 70 °C. The gas layer mold is used to cast 4-mm-thick chips of PDMS (1:10 mixture of Sylgard 184 cured overnight at 60 °C). After the inlet and outlet holes are punched in this latter chip, it is aligned and bonded by oxygen–plasma treatment to the flow layer mold. The two-layer device is then separated from the master, and the flow layer port holes are punched. To complete the microfluidic devices, the chips are bonded to a microscope cover glass by oxygen–plasma treatment.

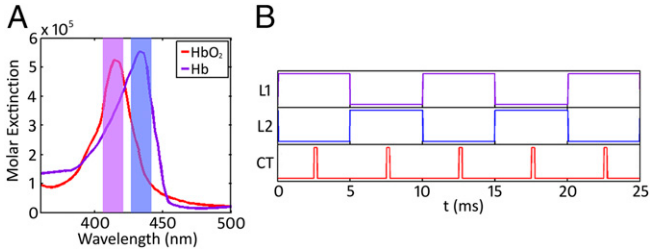

Fig. 6. Two-wavelength spectroscopy. (*A*) Absorption spectra of HbO_2 and Hb, where the two vertical bands represent the emission bandwidths of L1 and L2 ($\lambda = 410$ nm and $\lambda = 430$ nm, respectively; bandwidth FWHM = 20 nm). (*B*) Electronic signals generated by an Arduino Microcontroller driving the two LEDs (L1 and L2) and the camera trigger (CT).

Sample Preparation. Whole blood from healthy donors was obtained from an outside supplier (Research Blood Components). Blood was collected in an EDTA vacutainer, shipped on ice, rinsed with PBS, and spun down at 400 × *g* for 10 min to remove the plasma. To the remaining cells, 247.5 mL 40% BSA in PBS, 12 mL 20% (wt/vol) AB9 in PBS, 3 mL water, and 27.6 mL 10× PBS were added to produce a final osmotic pressure of 272 mOsm unless otherwise noted and an RBC concentration diluted 60× relative to whole blood. Cells were then loaded into microfluidic channels and measured as a function of ppO_2.

Two-Wavelength Spectroscopy. To differentiate between HbO_2 and Hb, we illuminate with two blue LEDs (L1: $\lambda = 410$ nm; L2: $\lambda = 430$ nm; bandwidth FWHM = 20 nm). The absorption spectra of HbO_2 and Hb are shown in Fig. 6*A* (21). From the absorption spectra of each species and the power spectral density of each blue LED, we can evaluate the absolute mass of both states of Hb. The values of the Hb mass for the two species are calculated by solving the system of equations:

$$E_{410} = e^{o}_{410} M_o + e^{d}_{410} M_d \quad \text{[1a]}$$

and

$$E_{430} = e^{o}_{430} M_o + e^{d}_{430} M_d, \quad \text{[1b]}$$

where M_o and M_d are the masses of HbO_2 and Hb, and $e^{o/d}_{410/430}$ is the molar extinction coefficient for HbO_2/Hb at 410/430 nm. The region in which the cell is present is segmented using an image processing routine based on an automatic Otsu's threshold evaluation: $E_{410/430} = A_{410/430} \cdot pa \cdot mw$, where A is the Hb absorbance at the two wavelengths defined as $\ln(I_{cell}/I_{ref})$, where I_{cell} is the segmented image of the cell, I_{ref} is an image when there is not a cell in the field of view, pa is the area of the segmented region containing the cells, and mw is the molecular weight of Hb (21).

We note that we observe uncalibrated saturation values that range from ~80% at 21% ppO_2 to 0% at 0% ppO_2. We believe that the saturation at 21% ppO_2 should be 100% and that our measurement is slightly biased by a small amount of residual optical scattering. To conform to this expectation, we have multiplied every cell saturation value by 1.28. We also note that, although the measured absorbance values are always positive, the resulting M_o values can be less than zero at 0% ppO_2 because of a small amount of measurement noise.

Cells are imaged through a microscope objective (40×, N.A. = 0.75; Olympus UPlanFLN) onto a color camera (640 × 480, pixel size = 7.4 μm; AVT Pike). The Bayer filter itself allows the independent acquisition of the red and blue signals. To separate the information carried by the absorption of Hb at 410 and 430 nm, the two LEDs are alternately triggered by an electronic signal (frequency = 100 Hz) generated by an Arduino Microcontroller (L1 and L2) (Fig. 6*B*). The same circuit generates the trigger signal for the camera (camera trigger) at double the frequency, enabling the capture of each color image in consecutive frames. The system allows a throughput of ~1,000 cells per minute.

1. Bianconi E, et al. (2013) An estimation of the number of cells in the human body. *Ann Hum Biol* 40(6):463–471.
2. Hill AV (1910) The possible effects of the aggregation of the molecules of haemoglobin on its dissociation curves. *J Physiol* 40:4–7.
3. Steinberg MH, Forget BG, Higgs DR, Weatherall DJ (2009) *Disorders of Hemoglobin: Genetics, Pathophysiology, and Clinical Management* (Cambridge Univ Press, Cambridge, United Kingdom).
4. Huh D, et al. (2010) Reconstituting organ-level lung functions on a chip. *Science* 328(5986):1662–1668.
5. Grosberg A, Alford PW, McCain ML, Parker KK (2011) Ensembles of engineered cardiac tissues for physiological and pharmacological study: Heart on a chip. *Lab Chip* 11(24):4165–4173.
6. Sung JH, Kam C, Shuler ML (2010) A microfluidic device for a pharmacokinetic-pharmacodynamic (PK-PD) model on a chip. *Lab Chip* 10(4):446–455.

7. Kim HJ, Huh D, Hamilton G, Ingber DE (2012) Human gut-on-a-chip inhabited by microbial flora that experiences intestinal peristalsis-like motions and flow. *Lab Chip* 12(12):2165–2174.
8. Wood DK, Soriano A, Mahadevan L, Higgins JM, Bhatia S (2012) A biophysical indicator of vaso-occlusive risk in sickle cell disease. *Sci Transl Med* 4(123):123ra26.
9. Polinkovsky M, Gutierrez E, Levchenko A, Groisman A (2009) Fine temporal control of the medium gas content and acidity and on-chip generation of series of oxygen concentrations for cell cultures. *Lab Chip* 9(8):1073–1084.
10. Rexius-Hall ML, Mauleon G, Malik AB, Rehman J, Eddington DT (2014) Microfluidic platform generates oxygen landscapes for localized hypoxic activation. *Lab Chip* 14(24):4688–4695.
11. Abbyad P, Tharaux PL, Martin JL, Baroud CN, Alexandrou A (2010) Sickling of red blood cells through rapid oxygen exchange in microfluidic drops. *Lab Chip* 10(19): 2505–2512.
12. Du E, Diez-Silva M, Kato GJ, Dao M, Suresh S (2015) Kinetics of sickle cell biorheology and implications for painful vasoocclusive crisis. *Proc Natl Acad Sci USA* 112(5):1422–1427.
13. Schonbrun E, Malka R, Di Caprio G, Schaak D, Higgins JM (2014) Quantitative absorption cytometry for measuring red blood cell hemoglobin mass and volume. *Cytometry A* 85(4):332–338.
14. James V, Goldstein DJ (1974) Haemoglobin content of individual erythrocytes in normal and abnormal blood. *Br J Haematol* 28(1):89–102.
15. Shapiro HM, et al. (1976) Combined blood cell counting and classification with fluorochrome stains and flow instrumentation. *J Histochem Cytochem* 24(1):396–401.
16. Grover WH, et al. (2011) Measuring single-cell density. *Proc Natl Acad Sci USA* 108(27): 10992–10996.
17. Rappaz B, et al. (2008) Comparative study of human erythrocytes by digital holographic microscopy, confocal microscopy, and impedance volume analyzer. *Cytometry A* 73(10):895–903.
18. Tycko DH, Metz MH, Epstein EA, Grinbaum A (1985) Flow-cytometric light scattering measurement of red blood cell volume and hemoglobin concentration. *Appl Opt* 24(9):1355–1365.
19. Mir M, Tangella K, Popescu G (2011) Blood testing at the single cell level using quantitative phase and amplitude microscopy. *Biomed Opt Express* 2(12):3259–3266.
20. Park Y, Yamauchi T, Choi W, Dasari R, Feld MS (2009) Spectroscopic phase microscopy for quantifying hemoglobin concentrations in intact red blood cells. *Opt Lett* 34(23): 3668–3670.
21. Prahl S (1998) *Tabulated Molar Extinction Coefficient for Hemoglobin in Water*. Available at omlc.org/spectra/hemoglobin/summary.html. Accessed May 10, 2015.
22. Lee JY, et al. (2012) Absorption-based hyperspectral imaging and analysis of single erythrocytes. *IEEE J Sel Top Quantum Electron* 18(3):1130–1139.
23. Wang L, Maslov K, Wang LV (2013) Single-cell label-free photoacoustic flowoxigraphy in vivo. *Proc Natl Acad Sci USA* 110(15):5759–5764.
24. Ellis CG, Ellsworth ML, Pittman RN (1990) Determination of red blood cell oxygenation in vivo by dual video densitometric image analysis. *Am J Physiol* 258(4 Pt 2): H1216–H1223.
25. Peterson DR, Bronzino JD (2014) *Biomechanics: Principles and Practices* (CRC, Boca Raton, FL), Chap 19, p 7.
26. Schonbrun E, Di Caprio G, Schaak D (2013) Dye exclusion microfluidic microscopy. *Opt Express* 21(7):8793–8798.
27. Carreau A, El Hafny-Rahbi B, Matejuk A, Grillon C, Kieda C (2011) Why is the partial oxygen pressure of human tissues a crucial parameter? Small molecules and hypoxia. *J Cell Mol Med* 15(6):1239–1253.
28. Dong H, Qin S, Zhou HX (2010) Effects of macromolecular crowding on protein conformational changes. *PLOS Comput Biol* 6(7):e1000833.
29. Benesch R, Benesch RE (1967) The effect of organic phosphates from the human erythrocyte on the allosteric properties of hemoglobin. *Biochem Biophys Res Commun* 26(2):162–167.
30. Haidas S, Labie D, Kaplan JC (1971) 2,3-diphosphoglycerate content and oxygen affinity as a function of red cell age in normal individuals. *Blood* 38(4):463–467.
31. Steinberg MH, Chui DHK, Dover GJ, Sebastiani P, Alsultan A (2014) Fetal hemoglobin in sickle cell anemia: A glass half full? *Blood* 123(4):481–485.
32. Kaoui B, Biros G, Misbah C (2009) Why do red blood cells have asymmetric shapes even in a symmetric flow? *Phys Rev Lett* 103(18):188101.